Structure and structural transition of chiral domains in oligo(p-phenylenevinylene) assembly investigated by scanning tunneling microscopy

Qing Chen[a,b], Ting Chen[a], Dong Wang[a], Hui-Biao Liu[a], Yu-Liang Li[a], and Li-Jun Wan[a,1]

[a]Beijing National Laboratory for Molecular Sciences, Institute of Chemistry, Chinese Academy of Sciences, Beijing 100190, China; and [b]Graduate University of Chinese Academy of Sciences, Beijing 100064, China

Communicated by Chunli Bai, The Chinese Academy of Sciences, Beijing, China, January 5, 2010 (received for review June 20, 2009)

OPV3-CHO molecules are employed to prepare assembly on highly oriented pyrolytic graphite, and the so-prepared assembly is investigated by scanning tunneling microscopy. In the assembly chiral domains are observed with various structures such as linear and windmill. The chiral structural formation, stability, transition, and possible unification are intensively studied. After thermal annealing, linear structure was the only structure. To achieve a unified assembly with a single structure, an efficient method is proposed by coadsorption of OPV3-CHO with selected molecules. For example, an assembly with side-by-side helix structure is formed by a simple coadsorption of OPV3-CHO with alkyl bromide ($C_nH_{2n+1}Br$, $n = 15–18$). The experiments by cocrystallization of OPV3-CHO/$C_nH_{2n+1}X$ (X = Cl, Br, and I) show the important role of halogen bonding in formation of the uniform structure. The results are significant in understanding the intermolecular noncovalent interactions that dominate the surface structure and chirality.

coadsorption | halogen bonding | surface chirality

Understanding the formation and structural transition of molecular nanostructure is an important issue in chemistry, molecular science, and nanodevice fabrication. Among various molecular nanostructures, two-dimensional surface chirality is a property of asymmetry and of great interest in fundamental research and industrial application such as life genesis, nonlinear optics, enantioselective heterogeneous catalysis, and surface modification (1–3). With atomic resolution, scanning tunneling microscopy (STM) is powerful in surface chirality study (4–7). From absolute chirality determination to chiral structure fabrication with chiral molecules or achiral molecules on a solid surface, a few results have been reported (8–13). Xu et al. directly observed the chirality of (*R*)- and (*S*)-2-phenylpropionamide molecules on Cu(111) in solution by using electrochemical STM (14). De Feyter et al. studied solvent-induced homochirality in self-assembled monolayers of achiral molecules. The chirality of the solvent directs the macroscopic chirality of the monolayer (15). After these results, we focus on the current challenge in surface chirality, which includes understanding the underlying driving force for the chiral formation, amplification, transition, and controlling the chiral structure.

Recently, oligo(p-phenylenevinylene) (OPV) and its derivatives have attracted a lot of attention because of their advanced optical and electronic properties and possible application in organic electronic devices (16–18). In the present report, an aldehyde-substituted OPV molecule (OPV3-CHO, Scheme 1) is used as a model compound to study its structure on a solid surface. It is found that achiral OPV3-CHO can form chiral domains on highly oriented pyrolytic graphite (HOPG). The OPV3-CHO adlayer is investigated by STM including structural formation, stability, transition, and possible unification of the chiral domains. The OPV3-CHO chiral domains appear in linear and windmill structures. These diversiform chiral organizations can be unified into one chiral structure after thermal annealing. An effective way is proposed to change the chiral structure by cocrystallization of OPV3-CHO with other molecules like that used in molecular engineering, surface science, and supramolecular chemistry (19–21). Here we demonstrate that with coadsorption of OPV3-CHO with alkyl bromides, diversiform chiral structures can be unified into one chirality. A series of alkyl derivatives including chloride, iodide, and alcohol are used. The effect of halogen bonding in the coadsorption is well studied. The results on surface chirality of OPV3-CHO will be significant in the understanding of surface molecular chirality and provide a possible route to control two-dimensional chiral structures.

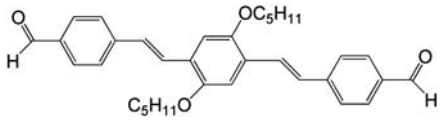

Scheme 1. Chemical structure of OPV3-CHO.

Results and Discussion

Multiple Chiral Structures of OPV3-CHO. Fig. 1 is a typical large-scale STM image of an OPV3-CHO adlayer on HOPG. The adlayer is composed of three main domains denoted with I, II, and III, respectively, and the domain boundaries are illustrated by white dashed lines. The three domains represent three kinds of chiral patterns: windmill in I, chiral linear in II, and dense windmill in III. The large-scale STM images of the three labeled domains are shown in Fig. S1.

Windmill Structure. Fig. 2*A* and *B* are the high-resolution images showing the details of the windmill structure. It is clearly seen from the images that the adlayer consists of bright rods and four bright rods form a windmill-like tetramer as the basic unit of the molecular assembly. Each bright rod is measured to be *ca.* 2.0 nm in its length, in agreement with the length of conjugated backbone of the OPV3-CHO molecule. Therefore, one bright rod in the image is corresponding to an OPV3-CHO molecule. The rotating direction of these windmills is clockwise in Fig. 2*A* and counterclockwise in Fig. 2*B*, denoted with "*R*" and "*S*," respectively. The schematic illustration for the different windmill-like unit is superimposed in Fig. 2*A* and *B* by blue arrows and white bold lines. A homochiral assembly in a domain can be recognized. In addition, the dodecyloxy chains of the molecules can be clearly observed in the space between these tetramers. All of the chains interdigitate each other and form a close-packed adlayer. On the basis of the molecular orientation and adlayer

Author contributions: Q.C. and L.-J.W. designed research; Q.C. performed research; H.-B.L. and Y.-L.L. contributed new reagents; Q.C., T.C., D.W., and L.-J.W. analyzed data; and Q.C., D.W., and L.-J.W. wrote the paper.

The authors declare no conflict of interest.

[1]To whom correspondence should be addressed. E-mail: wanlijun@iccas.ac.cn.

This article contains supporting information online at www.pnas.org/cgi/content/full/1000120107/DCSupplemental.

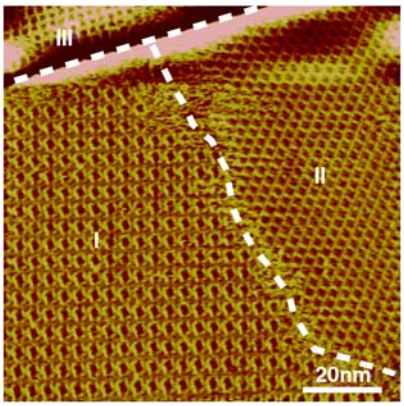

Fig. 1. Large-scale STM image of the OPV3-CHO adlayer on the HOPG surface with three chiral patterns. $V_{bias} = 567$ mV; $I_t = 606$ pA.

symmetry, unit cells of the windmill structure are outlined in Fig. 2*A* and *B* with molecular models. Although two unit cells are with the same parameters of $a = b = 3.8 \pm 0.1$ nm and $\alpha = 90°$, the windmills are in a chiral symmetry. The structural models are tentatively proposed in Fig. 2*C* and *D*. In the models, four molecules form a tetramer in a configuration of clockwise or counterclockwise windmill architecture.

A careful observation reveals that there are depressions in Fig. 2*A* and *B* as indicated by **A** with a red square. The depression is located in the center of a tetramer/windmill, consisting of four OPV3-CHO molecules. With theoretical simulation and calculation, it is understood that four aldehydes interact with hydrogen atoms of phenyls in the neighboring molecules and form H bondings with an average distance of 3.2 nm. The details are illustrated in the *Insets* of Fig. 2*C* and *D*. On the other hand, OPV3-CHO molecules are flat-lying on the HOPG surface with a parallel orientation. Alkyl chains also adsorb on the surface and interdigitate each other forming van der Waals (vdW) interaction between the dodecyloxy chains in molecular tetramers and between molecules and the substrate. The hydrogen bonding and vdW force should be responsible for the well-defined two-dimensional adlayer of OPV3-CHO on the HOPG surface.

Chiral Linear Structure. Chiral linear structure is carefully examined by high-resolution STM imaging. Fig. 3*A* and *B* are the typical images recorded in the linear chiral area. The STM images are composed of bright rods. Each rod in the image corresponds to an OPV3-CHO molecule. The molecules adsorb on the HOPG surface with parallel orientation and all alkyl chains interdigitate with each other. The rods position side by side and form linear rows as indicated by the white arrows. The structural details are denoted by the superimposed molecular models. Intriguingly, although the molecular arrangement is the same in the images of Fig. 3*A* and *B*, the molecular orientation is in mirror symmetry with chirality. A deformed windmill can also be determined as indicated in the image. The assembly chirality in Fig. 3*A* and *B* can be decided by the rotation of the deformed windmills as *S* and *R*, respectively. *R* is for clockwise, and *S* is for counterclockwise. The unit cells are outlined in the two images with the same parameters of $a = 2.3 \pm 0.1$ nm, $b = 3.0 \pm 0.1$ nm and $\alpha = 80 \pm 2°$ but different chirality. The tentative models as well as possible H bondings are shown in Fig. 3*C* and *D*. The average distance of these H bondings is 3.3 nm, and the angle is 160°. A single molecular line combined by the H bondings is highlighted and shown clearly in the red frame.

Dense Windmill Structure. The structure in domain III of Fig. 1 is a dense windmill-like structure. The high-resolution STM images from the dense windmill structure are shown in Fig. 4*A* and *B*. The two images are in chirality. Similar to the image feature in Figs. 2 and 3, each molecule appears in a bright rod. Each rod can be resolved as three conjoint dots in Fig. 4*B*, consistent with the molecular structure of three benzene rings in OPV3-CHO. Four molecules form a windmill-like unit. Different from the structure in Fig. 2, every two windmills can share one molecule as a common blade. Compared with the windmill structure in Fig. 2, the arrangement of the windmills in Fig. 4 is denser. From the intermolecular distance and molecular arrangement, it can be

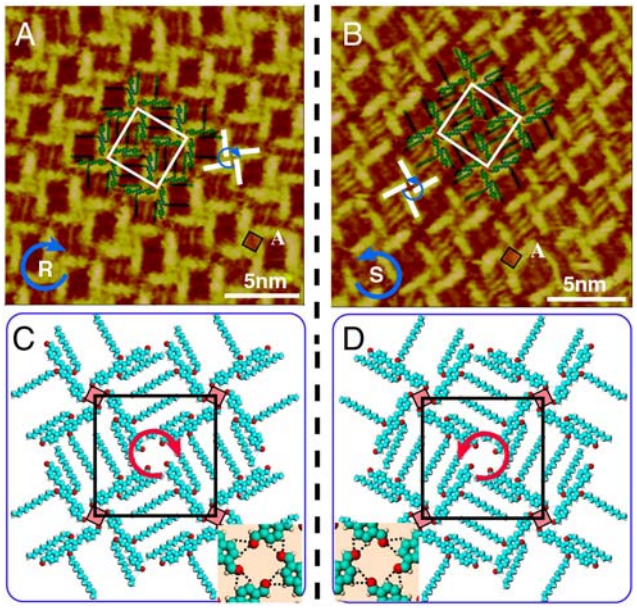

Fig. 2. Self-assembly of chiral windmill structure. (*A*) and (*B*) High-resolution STM images of windmill structure with clockwise and counterclockwise fashion. $V_{bias} = 635$ mV and $I_t = 640$ pA for (*A*), and $V_{bias} = 635$ mV and $I_t = 646$ pA for (*B*). (*C*) and (*D*) Structural models for adlayers in (*A*) and (*B*), respectively. The *Insets* in (*C*) and (*D*) show the possible H bondings in area *A* indicated by a red square.

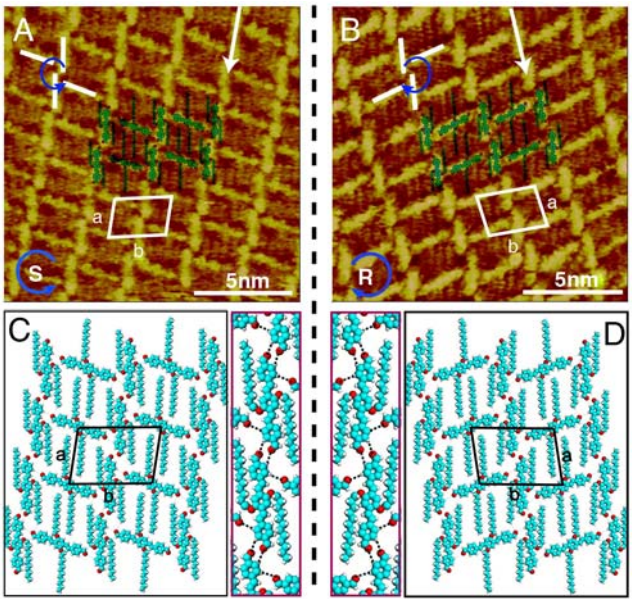

Fig. 3. Self-assembly of chiral linear structure. (*A*) and (*B*) High-resolution STM images of chiral linear structure with counterclockwise and clockwise fashion. $V_{bias} = 774$ mV and $I_t = 416$ pA for (*A*), and $V_{bias} = 750$ mV, $I_t = 500$ pA for (*B*). (*C*) and (*D*) Structural models for adlayers in domain *S* and *R*.

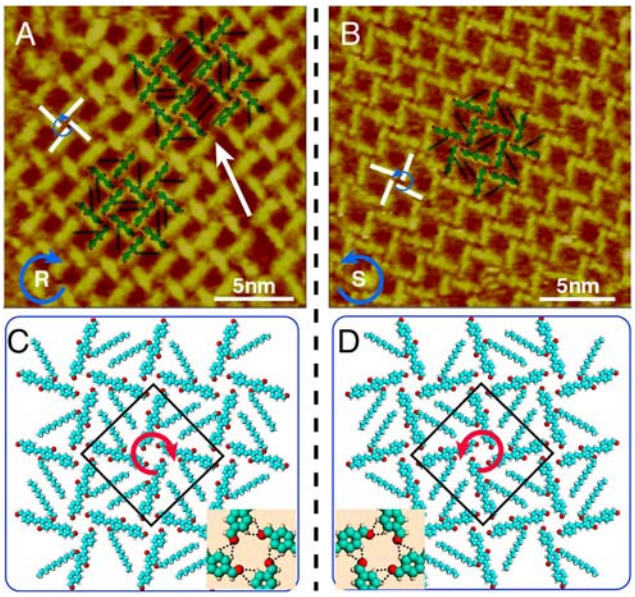

Fig. 4. Self-assembly of dense windmill structure. (*A*) and (*B*) High-resolution STM images showing clockwise and counterclockwise fashion. $V_{bias} = 624$ mV and $I_t = 653$ pA for (*A*), and $V_{bias} = 648$ mV and $I_t = 660$ pA for (*B*). (*C*) and (*D*) Structural models for adlayers in domain *R* and *S*. One dodecyloxy chain in a molecule pointing out from the HOPG surface is omitted in the models.

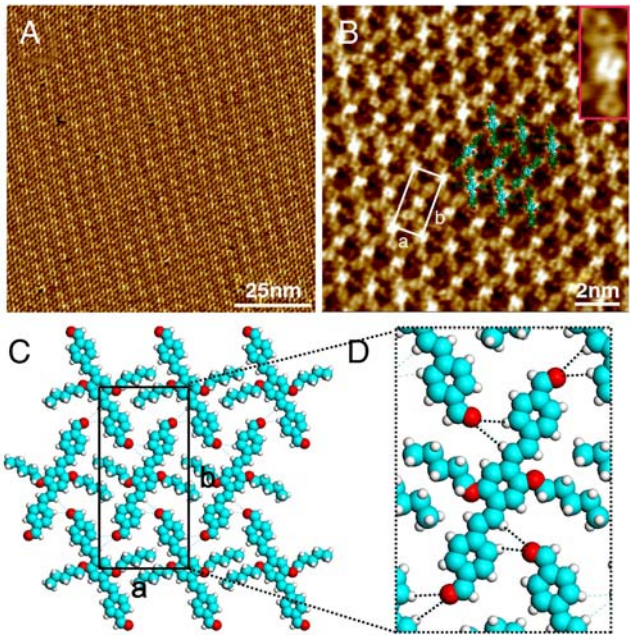

Fig. 5. Self-assembly of OPV3-C5 on HOPG. (*A*) Large-scale STM image. $V_{bias} = 670$ mV; $I_t = 655$ pA. (*B*) High-resolution STM image. $V_{bias} = 670$ mV; $I_t = 712$ pA. The *Inset* shows the details of a molecule. (*C*) Structural model for (*B*). (*D*) Calculated H bondings in the assembly.

found that only one dodecyloxy chain adsorbs on the HOPG surface and another chain in an OPV3-CHO molecule points out to the air (10). It is noted that a domain boundary appears in Fig. 4*A* as indicated by an arrow. However, the handedness of the windmills is the same in the neighboring domains. On the basis of the above analysis, the structural models are proposed in Fig. 4*C* and *D* for *a* and *b*, respectively. Unit cells with a parameter of $a = b = 3.2 \pm 0.1$ nm and $\alpha = 90 \pm 2°$ are outlined in the models. Because of the limited space, only half of alkyl chains are proposed to lie on surface. The possible H bondings in a windmill are proposed in the *Insets* of Fig. 4*C* and *D* for chiral domain *R* and *S*, respectively. The parameters of the H bonds are similar to those in windmill structure in Fig. 2.

Besides chiral domains, achiral domains are also observed occasionally and called achiral linear structure (Fig. S2). Compared with the chiral linear structure in Fig. 3, OPV3-CHO molecules are assembled alternatively along the molecular row, resulting in a racemic organization.

To understand the relationship between molecular chemical structure and self-assembly structure on the HOPG surface, we have studied the assemblies formed with OPV4-CHO and OPV3-C5. It is found that OPV4-CHO molecules form only one windmill-like structure on the HOPG surface (22). In another parallel experiment, the self-assembly of OPV3-C5, with a short alkyl chain, was also studied. Fig. 5 is a typical STM image showing the adlayer of OPV3-C5 on the HOPG surface. It is seen that the molecules form an ordered assembly with their benzene rings parallel to the HOPG surface. The three benzene rings with depressions in a molecule are clearly revealed in Fig. 5*B* and in the *Inset* of Fig. 5*B*. A single molecule is highlighted to show more details. The alkyl chains interdigitate with each other and organize into a close-packed adlayer. The proposed structural model as well as possible hydrogen bondings is shown in Fig. 5*C* and *D*. A rectangular unit cell is defined with the parameters of $a = 1.5 \pm 0.1$ nm, $b = 3.1 \pm 0.1$ nm. For the H bondings, one is 2.9 Å, 154°; another is 3.5 Å, 164°. The structure is a totally new structure different from those in OPV4-CHO and OPV3-CHO. No windmill structure can be corresponded. The structure is achiral. Why can OPV3-CHO molecules form such diversiform structures? The main difference in the three molecules is the difference in length ratio of OPV backbones and side chains. The main interactions in OPV assembly are (*i*) vdW interaction from the interdigitation of alkyl chains and between molecule and the HOPG substrate and (*ii*) hydrogen bondings existing between aldehydes and H atoms of phenyls. The structure formed by OPV molecules is dependent on the balance of these interactions. For OPV3-CHO, the length of the backbone and side chain is ~2.0 nm and ~1.5 nm, respectively. This length ratio and two aldehydes make diversiform structures possible. For OPV4-CHO, because the backbones become longer to ~2.5 nm, the unit cell expands, too. Accordingly, only the dense windmill structure is obtained in the self-assembly of OPV4-CHO. If the backbones of OPV4-CHO were similar to OPV3-CHO to form more patterns like chiral linear structure, windmill structure, and achiral linear structure, the dodecyloxy chains would be too short to get interdigitated, and thus none of these patterns would be energetically stable. For OPV3-C5, although the backbone is the same as that in OPV3-CHO, the alkyl chain is shorter. The alkyl chains can extend on the HOPG surface without rotation and well interdigitate each other. The interdigitation of alkyl chains, hydrogen bondings among aldehydes, and hydrogen atoms in backbones of OPV3-C5 molecules and the interaction between the molecule and HOPG substrate stabilize a dense-packed assembly. Therefore, owing to the difference in molecular structure, OPV3-CHO presents multiple structures, whereas OPV4-CHO and OPV3-C5 lack the structural diversity.

Annealing Effect on Chiral Transition. Thermal annealing is an efficient way to control surface structure, including chirality (23). Fig. 6*A* is an STM image obtained after heating the adlayer on HOPG at *ca.* 80 °C. This image shows five domains, and all of them are chiral linear structure. It is indicated that thermal treatment makes molecule assembly structures transfer from windmill structure, dense windmill structure, and achiral linear structure into chiral linear structure. In other words, three chiral structures and one achiral structure are uniformed into one chiral

structure. The high-resolution STM image in Fig. 6*B* confirms that the uniform chiral structure is chiral linear structure.

We have calculated surface coverage of these structures and summarized in Table 1. The coverage of the assemblies increases in an order of achiral linear structure, windmill structure, chiral linear structure, and dense windmill structure. Although dense windmill structure has the highest coverage among these structures, it also becomes disordered and evolves into chiral linear structure. Note that each OPV3-CHO molecule in a dense windmill assembly has only one side chain lying on the surface with another chain pointing out to air. The consequence is that chiral linear structure has both high coverage and strong supramolecular interactions. Therefore, this structure is the most thermodynamically stable one. Intriguingly, when the cocrystallization structure of OPV3-CHO/alkyl bromide (*vide post*) is heated, it is found that composite structures collapse and OPV3-CHO forms a chiral linear structure again. The results further support the conclusion that the chiral linear structure is the thermodynamically favorable assembly for OPV3-CHO.

Structural Unification by Cocrystallization. Mixing the OPV molecule and alkyl bromide into cocrystallization is proven to be another efficient route to unify the multiple structures of OPV3-CHO. Fig. 7*A* is a typical large-scale STM image of OPV3-CHO/$C_{18}H_{37}Br$ on HOPG. The equal distant bright lines are seen to distribute orderly on the surface. In the higher resolution STM image of Fig. 7*B*, it is found that the bright lines consist of short rods, i.e., backbones of OPV3-CHO, arranged in a linear helix fashion. The helix structure contains two enantiomers indicated by *R* and *S*. The domain boundary is illustrated by a white dashed line. As a transition, one OPV3-CHO molecule, indicated by the dashed circle, changes its assembly orientation and connects two chiral enantiomers.

In Fig. 7*B*, the dark area between bright molecular rows is attributed to alkyl chains (22, 24). Two kinds of alkyl chains are found between the molecular rows. One has a length of *ca.* 1.5 nm, corresponding to the dodecyloxy chains of OPV3-CHO indicated by red ellipses in the image. Another, located between the dodecyloxy chains of OPV3-CHO, is *ca.* 2.5 nm in length illustrated with blue ellipses, consistent with the length of the $C_{18}H_{37}Br$ molecule (24). There are two $C_{18}H_{37}Br$ molecules in every rectangular area surrounded by dodecyloxy chains, although it is difficult to determine the orientation of $C_{18}H_{37}Br$ (24, 25). Considering the halogen bonding between oxygen and bromide (26, 27), the two $C_{18}H_{37}Br$ molecules oriented oppositely in order to get close to the oxygen atoms of aldehyde groups. A rectangle unit cell is outlined with the lattice constants of $a = 1.7 \pm 0.1$ nm, $b = 3.9 \pm 0.1$ nm, $\alpha = 90 \pm 2°$. On the basis of the above analysis, the proposed models for the two enantiomers are shown in Fig. 7*C* and *D*. It is concluded that $C_{18}H_{37}Br$ molecules coadsorb with OPV3-CHO molecules, and the multiple self-assembly structures disappear whereas a uniform chiral helix structure is formed.

Table 1. The coverage of four assembly structures of OPV3-CHO

Patterns	Achiral linear	Windmill	Chiral linear	Dense windmill
Coverage (nm^{-2})	0.254	0.277	0.29	0.32

Hydrogen bonding plays an important role in molecular structure formation and transition. However, halogen bonding is another noncovalent force between the halogen atom and Lewis base (28, 29). The halogen atom in a molecule acts as an electron acceptor and a negative site in the Lewis base as an electron donor. Halogen bonding also plays significant roles in a wide variety of biochemical phenomena such as protein-ligand complexation (30, 31). The significance of halogen bonding has been increasingly understood from the effort of both theoretical chemistry and crystal engineering (32–34). Through a series of STM experiments we have investigated the cocrystallization of OPV3-CHO with alkyl bromides and studied the possible roles of halogen bonding. First, we studied the adlayer structures of OPV mixed with alkyl bromides in different length. Alkyl bromides of $C_nH_{2n+1}Br$ ($n = 15$–20) are selected. Fig. S3 shows the high-resolution STM images of the cocrystallization of OPV3-CHO/$C_{17}H_{35}Br$ and OPV3-CHO/$C_{16}H_{33}Br$. Red and blue ellipses for dodecyloxy chains and alkyl bromides are superposed on the images to illustrate the composite structure. The structure of OPV3-CHO/$C_{17}H_{35}Br$ is similar to OPV3-CHO/$C_{18}H_{37}Br$. For $C_{16}H_{33}Br$, there are four $C_{16}H_{33}Br$ molecules in every rectangular area encircled by dodecyloxy chains. Two bromide atoms are close to the oxygen atoms of aldehydes, whereas the other two bromide atoms are close to the oxygen atoms of dodecyloxy chains. In addition, because the length of $C_{16}H_{33}Br$ is shorter, there is no noticeable void area between two dodecyloxy chains in the STM image. For $C_{19}H_{39}Br$ and $C_{20}H_{41}Br$, as Fig. S4 shows, cocrystallization is not observed but phase separation instead. OPV3-CHO molecules form windmill and chiral linear structures, whereas alkyl bromides form lamellar structures separately.

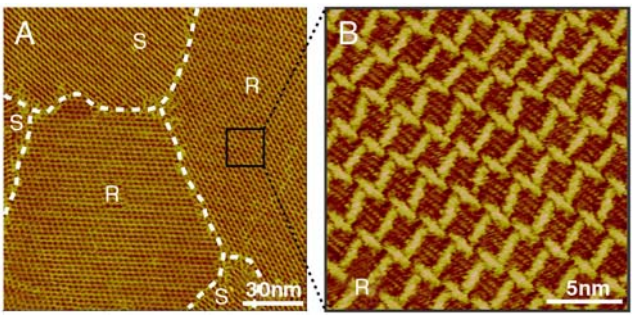

Fig. 6. The adlayer structure after annealing. (*A*) Large-scale STM image of the heated adlayer. $V_{bias} = 600$ mV; $I_t = 650$ pA. (*B*) High-resolution STM image. $V_{bias} = 635$ mV; $I_t = 646$ pA.

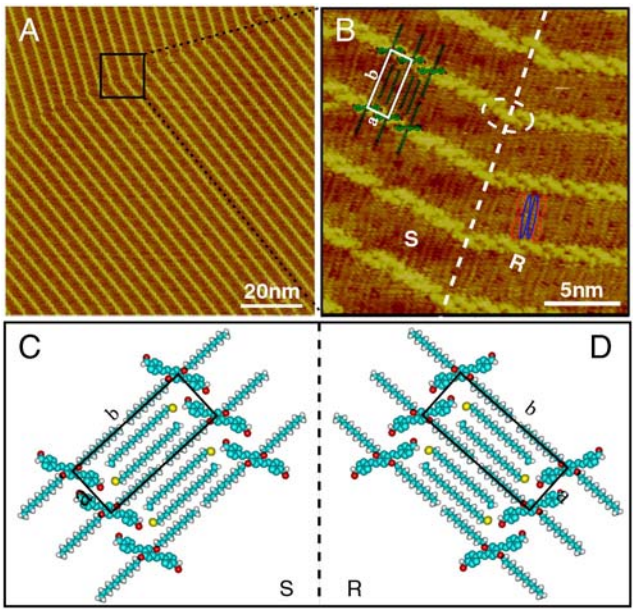

Fig. 7. Self-assembly of OPV3-CHO/$C_{18}H_{37}Br$ on HOPG. (*A*) Large-scale STM image. $V_{bias} = 784$ mV; $I_t = 580$ pA. (*B*) High-resolution STM image. $V_{bias} = 751$ mV; $I_t = 556$ pA. (*C*) and (*D*) Possible structural models for *R* and *S*.

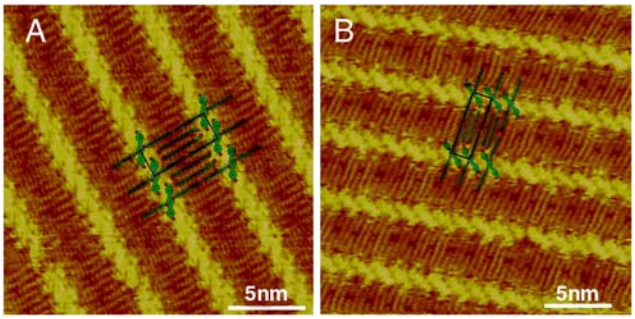

Fig. 8. High-resolution STM images of OPV3-CHO/$C_{18}H_{37}X$ (X = Cl and I). (*A*) OPV3-CHO/$C_{18}H_{37}Cl$: V_{bias} = 800 mV; I_t = 609 pA. (*B*) OPV3-CHO/$C_{18}H_{37}I$: V_{bias} = 750 mV; I_t = 620 pA.

On the other hand, when the alkyl bromide is shortened to $C_{15}H_{31}Br$, bicomponent linear structure of OPV3-CHO/$C_{15}H_{31}Br$ has also been observed. However, the composite cocrystallization is very unstable, and it is easy to be corrupted during STM scanning, and then OPV3-CHO rebuilds its own structure again (Fig. S4*c*). It is concluded that the alkyl bromides longer than $C_{18}H_{37}Br$ or shorter than $C_{15}H_{31}Br$ cannot form cocrystallization with OPV3-CHO. The most important reason should be the spatial match between these two molecular blocks.

Besides alkyl bromides, we have also tried other molecules such as alkane and alkyl alcohol. Interestingly, both $C_{18}H_{38}$ and $C_{18}H_{37}OH$ induce phase separation when mixed with OPV3-CHO, as shown in Fig. S5, suggesting that the halogen bond plays a significant role in the formation of the OPV3-CHO/bromides composite structure. Theoretical calculation finds that there is a positive charge, called a σ-hole, on halogen atoms' surfaces (35, 36). Therefore, the halogen atoms will interact with electronegative groups such as oxygen, nitrogen, hydroxyl, or carbonyl groups (26). The electrostatic potential map of OPV3-CHO shown in Fig. S6 calculated by the density functional theory (DFT) method reveals that the electrostatically negative positions locate at the oxygen of aldehydes and dodecyloxy chains. It is noteworthy that the introduction of alkyl halides in the assembly does not decrease the strength of the vdW force because all alkyl chains still keep the interdigitation arrangement and lie flat on the surface. However, the introduction changes the fashion in which aldehydes interact. For example, in the windmill structures of OPV3-CHO, molecules organize into a tetramer and aldehydes at the end of the backbone get together. But the aldehydes change to locate closer to the bromides in the structure of OPV3-CHO/$C_nH_{2n+1}Br$. As an electron donor, oxygen of the alkoxy group can also interact with the halogen atom. In the assembly of OPV3-CHO/$C_{16}H_{33}Br$, as the alkyl chain shortens, the OPV3 molecules pack loosely and four $C_{16}H_{33}Br$ molecules locate in the network surrounded by OPV3-CHO. Two of the four $C_{16}H_{33}Br$ molecules interact with oxygen of the alkoxy group, and the other two interact with oxygen of aldehydes.

With the understanding of the role of halogen bonding in the assembly, we have designed the experiments to use $C_{18}H_{37}Cl$ and $C_{18}H_{37}I$ to obtain cocrystallization structure with OPV3-CHO. As expected, the same cocrystallization structure as that of OPV3-CHO/$C_{18}H_{37}Br$ forms. The details of STM results are shown in Fig. 8. The bicomponent structures are similar to that in Fig. 7. The results demonstrate that halogen bonding helps greatly in the composite assembly of OPV3-CHO and halides.

Conclusion

With STM we have studied the structural stability, transition, and possible unification of the chiral domains in OPV3-CHO assembly. OPV3-CHO is found to form three chiral structures of linear, windmill, and dense windmill and an achiral structure. The polymorphism of the OPV3-CHO adlayer can be attributed to the appropriate length ratio of the backbone and side chain and two aldehyde substitutions. Thermal treatment makes these multiple structures evolve and unify to a single chiral linear structure. On the other hand, cocrystallization with alkyl halides (chloride, bromide, and iodide) in different alkyl lengths makes OPV3-CHO diversiform structures unify into one new helix chiral structure. The halogen bonding between the halogen atom of $C_nH_{2n+1}X$ (X = Cl, Br, and I) and oxygen of OPV3-CHO is proposed as one of the driving forces for the structural transition. The role of halogen bonding is systematically investigated including alkyl bromide with different chain lengths and different elements of the halogen group.

Materials and Methods

Chemicals and Substrate. Oligo(p-phenylenevinylene)s substituted by aldehydes at both ends (OPV3-CHO) is home-synthesized as reported before (37). 1-Bromoeicosane ($C_{20}H_{41}Br$; TCI), 1-Bromononadecane ($C_{19}H_{39}Br$; Fluka), 1-Bromooctadecane ($C_{18}H_{37}Br$; Aldrich), 1-Bromoheptadecane ($C_{17}H_{35}Br$; TCI), 1-Bromohexadecane ($C_{16}H_{33}Br$; Acros), 1-Bromopentadecane ($C_{15}H_{31}Br$; Acros), 1-Chlorooctadecane ($C_{18}H_{37}Cl$; Aldrich), 1-Iodooctadecane ($C_{18}H_{37}I$; TCI), octadecane ($C_{18}H_{38}$; Acros), and 1-octadecanol ($C_{18}H_{37}OH$; TCI) are used as received.

Molecular Adlayers and STM Measurements. A drop of acetone solution containing the OPV3-CHO molecule (<10^{-4} M) and OPV3/$C_nH_{2n+1}X$ (X = Br, Cl, I, H, and OH) mixture (1:3) is directly deposited onto a freshly cleaved, atomically flat HOPG surface. The former is used for the preparation of oligomer chiral assembly, and the latter for tuning structures. In all cases the acetone is evaporated thoroughly before STM measurement. STM experiments are performed with a NanoScope IIIa (Digital Instruments) at ambient conditions. The tunneling tips are prepared by mechanically cutting Pt/Ir wire (90/10).

Calculation. Theoretical calculations were performed with Materials Studio 3.1 by using DFT as implemented in the DMol3 package. With a maximum distance of 0.35 nm and a minimum angle of 120°, the possible H bondings in the supramolecular adlayer are calculated (38).

ACKNOWLEDGMENTS. This work was supported by the National Natural Science Foundation of China (Grants 20821003, 20821120291, and 20733004), the National Key Project on Basic Research (Grants 2006CB806100 and 2006CB932100), and the Chinese Academy of Sciences.

1. Bonello JM, Williams FJ, Lambert RM (2003) Aspects of enantioselective heterogeneous catalysis: Structure and reactivity of (S)-(-)-1-(1-naphthyl)ethylamine on Pt{111}. *J Am Chem Soc* 125:2723–2729.
2. Ernst KH (2006) Supramolecular surface chirality. *Top Curr Chem* 265:209–252.
3. Wang D, et al. (2005) Surface structure of heterogeneous catalysts: Cinchona and tartaric acid on solid surface. *Top Catal* 35:131–139.
4. Elemans J, De Cat I, Xu H, De Feyter S (2009) Two-dimensional chirality at liquid-solid interfaces. *Chem Soc Rev* 38:722–736.
5. Wan LJ (2006) Fabricating and controlling molecular self-organization at solid surfaces: Studies by scanning tunneling microscopy. *Acc Chem Res* 39:334–342.
6. Busse C, et al. (2007) Chiral ordering and conformational dynamics for a class of oligo-phenylene-ethynylenes on Au(111). *J Phys Chem B* 111:5850–5860.
7. Raval R (2009) Chiral expression from molecular assemblies at metal surfaces: Insights from surface science techniques. *Chem Soc Rev* 38:707–721.
8. Humblot V, Barlow SM, Raval R (2004) Two-dimensional organisational chirality through supramolecular assembly of molecules at metal surfaces. *Prog Surf Sci* 76:1–19.
9. Yuan Q-H, et al. (2008) Scanning tunneling microscopy investigation of a supramolecular self-assembled three-dimensional chiral prism on a Au(111) surface. *J Am Chem Soc* 130:8878–8879.
10. Chen T, et al. (2009) Linear dislocation turns chirality: A unique example of origination and amplification of chirality on an HOPG surface. *Chem Commun* 2649–2651.
11. Chen Q, et al. (2008) Structural selection of graphene supramolecular assembly oriented by molecular conformation and alkyl chain. *Proc Natl Acad Sci USA* 105:16849–16854.
12. Xu QM, et al. (2002) Adsorption mode of cinchonidine on Cu(111) surface. *J Am Chem Soc* 124:14300–14301.
13. Han MJ, et al. (2004) Absolute configuration of monodentate phosphine ligand enantiomers on Cu(111). *Anal Chem* 76:627–631.
14. Xu QM, et al. (2002) Discriminating chiral molecules of (R)-PPA and (S)-PPA in aqueous solution by ECSTM. *Angew Chem Int Edit* 41:3408–3411.
15. Katsonis N, et al. (2008) Emerging solvent-induced homochirality by the confinement of achiral molecules against a solid surface. *Angew Chem Int Edit* 47:4997–5001.

16. Schenning APHJ, et al. (2004) Towards supramolecular electronics. *Synthetic Met* 147:43–48.
17. Jonkheijm P, et al. (2004) pi-conjugated oligo-(p-phenylenevinylene) rosettes and their tubular self-assembly. *Angew Chem Int Edit* 43:74–78.
18. Ajayaghosh A, Praveen VK (2007) pi-organogels of self-assembled p-phenylenevinylenes: Soft materials with distinct size, shape, and functions. *Acc Chem Res* 40:644–656.
19. Li SS, et al. (2007) Control of supramolecular rectangle self-assembly with a molecular template. *J Am Chem Soc* 129:9268–9269.
20. Yoshimoto S, Honda Y, Ito O, Itaya K (2008) Supramolecular pattern of fullerene on 2D bimolecular "chessboard" consisting of bottom-up assembly of porphyrin and phthalocyanine molecules. *J Am Chem Soc* 130:1085–1092.
21. Wang L, et al. (2008) Nanopatterning of donor/acceptor hybrid supramolecular architectures on highly oriented pyrolytic graphite: A scanning tunneling microscopy study. *J Am Chem Soc* 130:13433–13441.
22. Chen Q, et al. (2009) Two dimensional OPV4 self-assembly and its coadsorption with alkyl bromide: From helix to lamellar. *Chem Commun* 3765–3767.
23. Rohde D, Yan CJ, Yan HJ, Wan LJ (2006) From a lamellar to hexagonal self-assembly of bis(4,4′-(m,m′-di(dodecyloxy)phenyl)-2,2′-difluoro-1,3,2-dioxaborin) molecules: A trans-to-cis-isomerization-induced structural transition studied with STM. *Angew Chem Int Edit* 45:3996–4000.
24. Chen Q, et al. (2008) STM investigation of the dependence of alkane and alkane (C18H38, C19H40) derivatives self-assembly on molecular chemical structure on HOPG surface. *Surf Sci* 602:1256–1266.
25. Cyr DM, et al. (1996) Functional group identification in scanning tunneling microscopy of molecular adsorbates. *J Phys Chem* 100:13747–13759.
26. Riley KE, Hobza P (2008) Investigations into the nature of halogen bonding including symmetry adapted perturbation theory analyses. *J Chem Theory Comput* 4:232–242.
27. Yang XY, et al. (2007) Halogen bonded two-dimensional supramolecular assemblies studied by high resolution scanning tunneling microscopy. *Chinese Sci Bull* 52:1856–1859.
28. Metrangolo P, Resnati G (2008) Chemistry—Halogen versus hydrogen. *Science* 321:918–919.
29. Metrangolo P, Neukirch H, Pilati T, Resnati G (2005) Halogen bonding based recognition processes: A world parallel to hydrogen bonding. *Acc Chem Res* 38:386–395.
30. Auffinger P, Hays FA, Westhof E, Ho PS (2004) Halogen bonds in biological molecules. *Proc Natl Acad Sci USA* 101:16789–16794.
31. Metrangolo P, et al. (2008) Halogen bonding in supramolecular chemistry. *Angew Chem Int Edit* 47:6114–6127.
32. Goebel M, et al. (2009) Chlorotrinitromethane and its exceptionally short carbon-chlorine bond. *Nat Chem* 1:229–235.
33. Riley KE, Merz KM (2007) Insights into the strength and origin of halogen bonding: The halobenzene-formaldehyde dimer. *J Phys Chem A* 111:1688–1694.
34. Muniappan S, Lipstman S, Goldberg I (2008) Rational design of supramolecular chirality in porphyrin assemblies: The halogen bond case. *Chem Commun* 1777–1779.
35. Murray JS, Lane P, Politzer P (2007) A predicted new type of directional noncovalent interaction. *Int J Quantum Chem* 107:2286–2292.
36. Mohajeri A, Pakiari AH, Bagheri N (2009) Theoretical studies on the nature of bonding in sigma-hole complexes. *Chem Phys Lett* 467:393–397.
37. Jiu TG, et al. (2007) Molecular modeling of poly(p-phenylenevinylene): Synthesis and photophysical properties of oligomers. *J Polym Sci A1* 45:911–924.
38. Liu Z, Wang G, Li Z, Wang R (2008) Geometrical preferences of the hydrogen bonds on protein-ligand binding interface derived from statistical surveys and quantum mechanics calculations. *J Chem Theory Comput* 4:1959–1973.